Progress In Electromagnetics Research C, Vol. 45, 237–249, 2013

NUMERICAL INVESTIGATIONS OF ULTRA WIDEBAND STACKED RECTANGULAR DRA EXCITED BY RECTANGULAR PATCH

Idris Messaoudene*, Abdelmadjid Benghalia, Mohamed A. Boughendjour, and Bilal Adjaoud

Laboratoire des Hyperfréquences et Semiconducteurs, Université de Constantine 1, Route d'Ain El Bey, Constantine 25000, Algerie

Abstract—In this paper, a numerical study of a new ultra wideband (UWB) dielectric resonator antenna (DRA) is presented. The proposed structure consists of two stacked dielectric resonators excited by rectangular patch and operated from 3 GHz to 11 GHz (an impedance bandwidth of 115%), covering the full UWB spectrum. The analysis is carried out using the Finite Difference Time Domain (FDTD) method and two commercial electromagnetic simulators. The numerical results are given and compared in terms of reflection coefficients, radiation pattern and gain. The computed FDTD results are in good agreement with those of simulations.

1. INTRODUCTION

The dielectric resonator antennas (DRAs) have become attractive to antenna engineers due to its several beneficial features, such as its small size, light weight, low loss, high radiation efficiency, and easy of excitation. The need of the high-data rate, in the recent communication devices, has forced the researchers to enhance the small antenna bandwidth. In the literature, several studies have been reported to achieve wide-bandwidth enhancement of DRAs suitable for wideband applications, as using stacked segment dielectric resonators (DRs) [1], stacked-embedded DRs [2], hybrid DRA [3], and special geometries of DR, such as conical [4], tetrahedral [5], elliptical [6], stair [7], H-shaped [8], and P-shaped [9]. Using these techniques, an impedance bandwidth range of 30–70% has been achieved.

Received 8 November 2013, Accepted 4 December 2013, Scheduled 4 December 2013

* Corresponding author: Idris Messaoudene (idris_messaoudene@yahoo.fr).

In the last decade, the Federal Communications Commission (FCC) allowed the use of the frequency band from 3.1 to 10.6 GHz for commercial applications. Many investigations have been reported to design adequate antennas for UWB spectrum. The proposed antennas are mainly based on planar monopoles with different shapes such as rectangular, circular, semi-elliptical, and trapezoidal forms [10–13] and on slot antennas, using a tuning stub with rectangular shape [14], circular shape [15], and fork-like shape [16]. Due to their advantages compared with metallic antennas, some research papers have recently proposed the dielectric resonator antennas to be one of the attractive candidate antennas for UWB applications, such as a half cylindrical dielectric resonator antenna [17], an A-shaped resonator [18], an inserted DRA excited by CPW [19], and a conical-shape DR with monopole antenna [20].

In this paper, we propose a new rectangular patch fed stacked dielectric resonator antenna. Compared to the existed stacked DRAs, the proposed design provides an impedance bandwidth more than 115% (between 3 GHz and 11 GHz), covering the UWB spectrum (3.1 GHz–10.6 GHz) and having an omni-directional radiation pattern. The FDTD method is used to analyze the proposed antenna, adopting the convolutional perfectly matched layers (CPML) as absorbing boundary conditions (ABCs). To check calculations, the numerical results are compared with those obtained from the Ansoft High Frequency Structure Simulator HFSS and CST Microwave Studio simulations.

The organization of the paper is as follow. The antenna's geometry, analytical study, and FDTD model are described in the next section. In Section 3, the numerical results are presented, compared, and discussed. Finally, a conclusion is drawn in Section 4.

2. ANTENNA CONFIGURATION AND ANALYSIS

2.1. Antenna Geometry

Figure 1 shows the geometry of the antenna structure under consideration. The proposed design comprised two stacked rectangular dielectric resonators (DR), with width a and length b, excited via microstrip transmission line, with length ls and width ws, printed on the top side of the subtrate. The lower DR (DR1) is made of Rogers RO4350 with permittivity $\varepsilon_{r1} = 3.66$ and height $d1$, the upper DR (DR2) has a relative permittivity $\varepsilon_{r2} = 10.2$ (Rogers RO3010) and height $d2$. The stacked DRs are mounted on $L \times W$ Rogers RT5880 substrate with permittivity $\varepsilon_{rs} = 2.2$, loss tangent of 0.0009, and thickness $h = 0.762$ mm. The ground plane is partially printed on

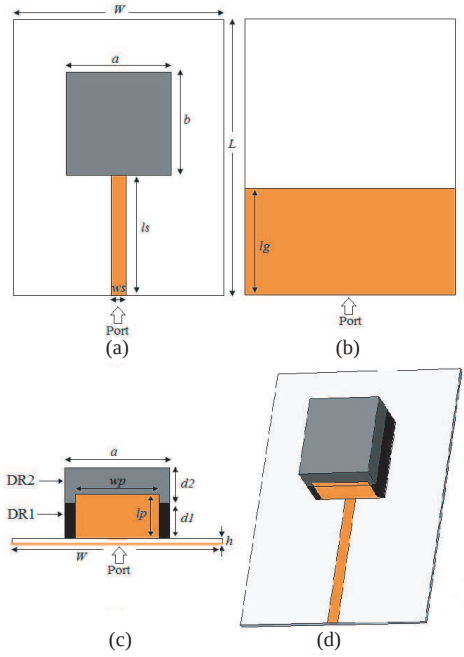

Figure 1. Geometry of the proposed structure; (a) Top view, (b) bottom view, (c) side view, (d) 3D view.

the bottom side of the substrate, with length *lg*. A rectangular patch, with length *lp* and width *wp*, adhered to the back side surface of the stacked resonators and connected to the microstrip line, is used as excitation mechanism, as illustrated in Figure 1. Table 1 summarizes the optimal parameters of the proposed antenna design.

Table 1. Optimal dimensions of the proposed antenna.

Parameter	L	W	a	b	$d1$	$d2$	wp	lp	Lg	h	ws	ls
Value (mm)	40	30	15	15	5.08	5.08	11	6.5	16	0.762	2.2	17.5

2.2. Analytical Study

According to [21], the proposed coupling technique, which uses a rectangular flat metallic strip connected to the microstrip line for the feeding mechanism, excites the Transverse Electric (TE_{mnp}) modes, where the lowest order mode is TE_{111}. By using the dielectric waveguide model (DWM) to analyse a rectangular DR antenna with

dimension a, $b > d$, the fields within the RDRA are obtained, as follows:

$$\begin{cases} H_x = \dfrac{k_x k_z}{j\omega\mu_0} \sin(k_x x)\cos(k_y y)\sin(k_z z) \\ H_y = \dfrac{k_y k_z}{j\omega\mu_0} \cos(k_x x)\sin(k_y y)\sin(k_z z) \\ H_z = \dfrac{k_x^2 + k_y^2}{j\omega\mu_0} \cos(k_x x)\cos(k_y y)\cos(k_z z) \\ E_x = k_y \cos(k_x x)\sin(k_y y)\cos(k_z z) \\ E_y = -k_x \sin(k_x x)\cos(k_y y)\cos(k_z z) \\ E_z = 0 \end{cases} \tag{1}$$

where

$$k_x^2 + k_y^2 + k_z^2 = \epsilon_r k_0^2$$

The resonant frequency f_0 is found by solving the following transcendental equation:

$$k_z \tan(k_z d/2) = \sqrt{(\epsilon_r - 1)k_0^2 - k_z^2} \tag{2}$$

where:

$$k_0 = 2\pi f_0, \quad k_x = m\pi/a, \quad k_y = n\pi/b$$

The subscripts m, n, and p represent the field variation in the x-, y-, and z-directions, respectively.

2.3. FDTD Solution

The Finite Difference Time Domain (FDTD) formulation for solving antenna problems is well known and reported in many previous investigations [22]. In this work, the 3-D FDTD algorithm with Cartesian grid is applied to analyze the proposed antenna. The space steps used in the FDTD simulation are Δx, Δy, and Δz. The time step used is Δt which satisfies the courant stability condition [23].

A simple source approximation is used to model the feed of the microstrip line [22]. A baseband Gaussian pulse of half-width $T = 3$ ps and time delay $t_0 = 5T$ is applied at the source plane. The width of the pulse and the time delay are chosen to suit the frequency bands of interest. Convolutional Perfectly Matched Layers (CPML) [24] absorbing boundary conditions (ABCs) were used to terminate the calculation space. The antenna under consideration is enclosed by eight CPML layers in all directions. Six cells are used in order to separate the structure and the CPML.

Starting from Amper's Law, the x-projection of the electric field in the CPML can be written in the form:

$$j\omega\varepsilon_x E_x + \sigma_x E_x = \frac{1}{s_y}\frac{d}{dy}H_z + \frac{1}{s_z}\frac{d}{dz}H_y \tag{3}$$

where S_i is the stretched-coordinate metrics proposed by Berenger, given by:

$$S_i = 1 + \frac{\sigma_i}{j\omega\varepsilon_0}, \quad i = x,\ y,\ \text{or}\ z \tag{4}$$

Then, the Equation (3) is transformed in the time domain, as follows:

$$\varepsilon_x \frac{d}{dt}E_x + \sigma_x E_x = \bar{S}_y(t) * \frac{d}{dy}H_z + \bar{S}_z(t) * \frac{d}{dz}H_y \tag{5}$$

where $\bar{S}_i(t)$ is the inverse Laplace transform of $\frac{1}{s_i}$ and * denotes the convolution.

The complex S_i is given by Kuzuoglu and Mittra as:

$$S_i = \kappa_i + \frac{\sigma_i}{\alpha_i + j\omega\varepsilon_0}, \quad i = x,\ y,\ \text{or}\ z \tag{6}$$

where α_i and σ_i are positive real and κ_i is real and ≥ 1.

And $\bar{S}_i(t)$ becomes:

$$\bar{S}_i(t) = \frac{\delta(t)}{\kappa_i} - \frac{\sigma_i}{a_i + \varepsilon_0\kappa_i^2} e^{-((\sigma_i/\varepsilon_0\kappa_i)+(\sigma_i/\varepsilon_0))t} u(t) \tag{7}$$

After the discretization of Equation (5) in the space and the time domain and using the recursive convolution, the implemented update equation of the x-electric component in the CPML is given by (for more details see [25]):

$$\begin{aligned}
&\varepsilon_x(i,j,k)\frac{E_x^{n+1}(i,j,k) - E_x^n(i,j,k)}{\Delta t} + \sigma_x(i,j,k)\frac{E_x^{n+1}(i,j,k) - E_x^n(i,j,k)}{2} \\
&= \frac{1}{k_y(i,j,k)}\frac{H_z^{n+\frac{1}{2}}(i,j,k) - H_z^{n+\frac{1}{2}}(i,j-1,k)}{\Delta y} \\
&\quad - \frac{1}{k_z(i,j,k)}\frac{H_y^{n+\frac{1}{2}}(i,j,k) - H_y^{n+\frac{1}{2}}(i,j,k-1)}{\Delta z} \\
&\quad + \psi_{exy}^{n+\frac{1}{2}}(i,j,k) - \psi_{exy}^{n+\frac{1}{2}}(i,j,k)
\end{aligned} \tag{8}$$

with:

$$\psi_{exy}^{n+\frac{1}{2}}(i,j,k) = \sum_{m=0}^{m=n-1} Z_{0ey}(m)\left(H_z^{n-m+\frac{1}{2}}(i,j,k) - H_z^{n-m+\frac{1}{2}}(i,j-1,k)\right) \tag{9}$$

$$\psi_{exy}^{n+\frac{1}{2}}(i,j,k) = \sum_{m=0}^{m=n-1} Z_{0ez}(m)\left(H_y^{n-m+\frac{1}{2}}(i,j,k) - H_y^{n-m+\frac{1}{2}}(i,j,k-1)\right) \tag{10}$$

where

$$Z_{0ei}(m) = a_{ei}e\left((\sigma_i/\kappa_i) + a_i\right)(m\Delta t/\varepsilon_0), \quad i = x,\, y,\, \text{or}\, z \tag{11}$$

$$a_{ei} = \frac{\sigma_i}{\sigma_i\kappa_i + \alpha_i\kappa_i^2}[e - ((\sigma_i/\kappa_i) + a_i)(\Delta t/\varepsilon_0)], \; i = x, y, \text{or}\, z \tag{12}$$

After the field distribution has been obtained, the radiation pattern can be calculated using the near-field to far-field transformation [25]. First of all, the equivalent electric and magnetic currents **J** and **M** on an imaginary surface, selected to enclose the proposed antenna, are calculated using the E and H field inside the structure. For example, Equation (13) shows the surface current J_y calculated in the frequency domain from the magnetic field H_x.

$$J_y(f) = H_x(f) = \sum_{n=1}^{N} H_x(n)e^{-2\pi f n\Delta t}\Delta t \tag{13}$$

Then, the resulting currents are used to compute vector potentials **A** and **F**, as shown by following equations

$$\mathbf{A} = \frac{\mu_0 e^{-jkR}}{4\pi R}\mathbf{N} \tag{14}$$

$$\mathbf{F} = \frac{\varepsilon_0 e^{-jkR}}{4\pi R}\mathbf{L} \tag{15}$$

with:

$$\mathbf{N} = \int \mathbf{J}_s e^{-jkr\cos(\psi)} ds \tag{16}$$

$$\mathbf{L} = \int \mathbf{M}_s e^{-jkr\cos(\psi)} ds \tag{17}$$

where $\mathbf{J}_s$ and $\mathbf{M}_s$ are the electric and magnetic surface currents, respectively.

Finally, the E and H far-fields components can be obtained from the vector potentials, as follows:

$$E_\theta = -\frac{jke^{-jkr}}{4\pi r}(L_\varphi + \eta_0 * N_\theta) \tag{18}$$

$$E_\varphi = \frac{jke^{-jkr}}{4\pi r}(L_\theta + \eta_0 * N_\varphi) \tag{19}$$

$$H_\theta = \frac{jke^{-jkr}}{4\pi r}\left(N_\varphi - \frac{L_\theta}{\eta_0}\right) \tag{20}$$

$$H_\varphi = -\frac{jke^{-jkr}}{4\pi r}\left(N_\theta + \frac{L_\varphi}{\eta_0}\right) \tag{21}$$

where η_0 is the wave impedance of free space.

Table 2 includes all parameters of the FDTD implementation. The simulation is performed for 5000 iterations to allow the input response become approximately zero.

Table 2. Parameters of FDTD model.

FDTD Parameters	Value
Δx (mm)	0.3
Δy (mm)	0.3
Δz (mm)	0.2
Δt (ps)	0.17
Number of Iteration	5000
Half-width of the Gaussian pulse T (ps)	3
Time delay t_0 (ps)	15
CPML in each direction	8

3. NUMERICAL RESULTS AND DISCUSSION

The numerical analysis was carried out using the CPML-FDTD implementation, the Ansoft HFSS, which utilizes Finite Element Method (FEM) in frequency domain, and the CST-MS based on Finite Integration Technique (FIT) in time domain. The numerical results are presented and compared in terms of reflection coefficients and radiation patterns.

3.1. Reflection Coefficient

Since the proposed antenna is a one port circuit, its scattering matrix has only one element, that S_{11} or the reflection coefficient given by the following formula:

$$S_{11}(f)_{\mathrm{dB}} = 20\log\left(\frac{V_{ref}(f)}{V_{inc}(f)}\right) \tag{22}$$

where $V_{ref}(f)$ is the Fourier transformed reflection voltage at the terminal plane and $V_{inc}(f)$ the Fourier transformed incident voltage at the same plane.

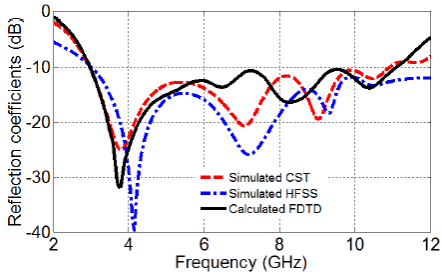

Figure 2. Calculated and simulated reflection coefficients of the proposed antenna.

The computed and simulated return losses of the proposed antenna are plotted together in Figure 2. It can be seen that the stacked DRA achieved an impedance bandwidth of; 115.7% from the FDTD implementation (from 3 GHz to 11.1 GHz for $S_{11} < -10$ dB), 128.5% (between 3 GHz and 12 GHz) for the HFSS simulation, and 113.2% (3–10.93 GHz) from the CST results. The proposed design allows the covering of the entire UWB spectrum band. The numerical results show a good agreement.

3.2. Radiation Characteristics

To get the radiation pattern characteristics, the Gaussian excitation is replaced by a sinusoidal function at the source plane, which given by

$$V(t) = \sin(2\pi f_i t) \tag{23}$$

where f_i takes three sampled frequencies (f_i = 3.5 GHz, 6.5 GHz, or 10 GHz).

Figures 3(a), (b), and (c) show the radiation pattern in the two main planes (the E and H-planes) of the DR antenna at 3.5 GHz, 6.5 GHz, and 10 GHz, respectively. It is observed that the proposed antenna has monopole-like patterns in the E-plane, while The H-plane radiation patterns are omni-directional through the entire resonant frequency band. It is noted that the far-field radiation pattern exhibits little deformation at 10 GHz because the effects of higher order modes. The FDTD computation results in term of far-field radiation patterns are in a very good agreement with those of HFSS simulation. Figure 4 shows the gain obtained from CST simulation versus frequency for the proposed antenna. It is found that the UWB antenna gain rages from 3 dB to 4.7 dB.

In addition, Figure 5 shows the simulated current distributions on the UWB antenna at 3.5 GHz, 6.5 GHz, and 10 GHz, respectively.

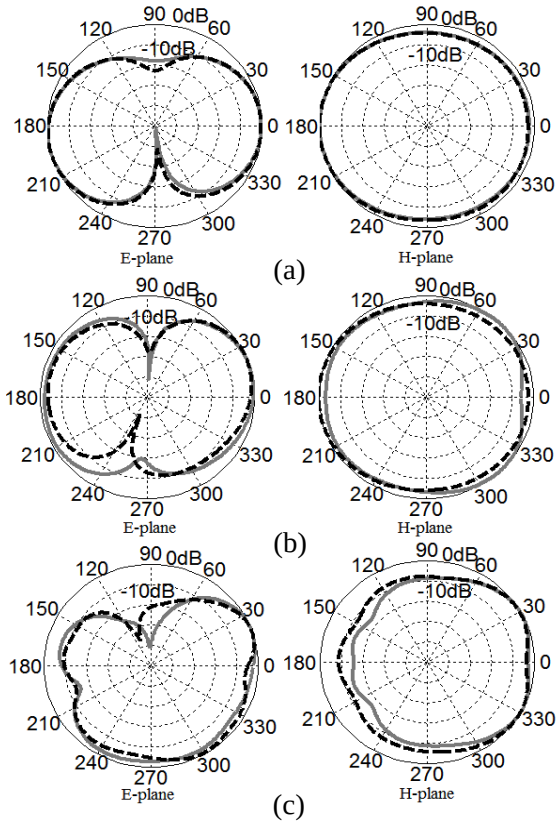

Figure 3. Radiation pattern of the UWB antenna at (a) 3.5 GHz, (b) 6.5 GHz, (c) 10 GHz; Note: light Solid lines for FDTD calculation and Dark dashed lines for HFSS simulation.

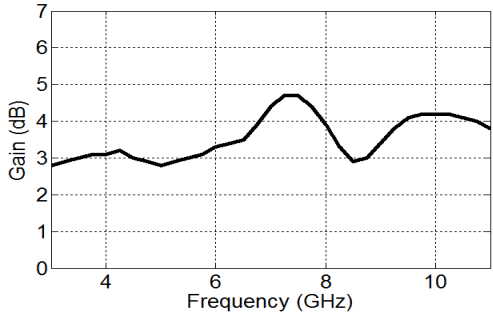

Figure 4. Simulated gain of the proposed antenna.

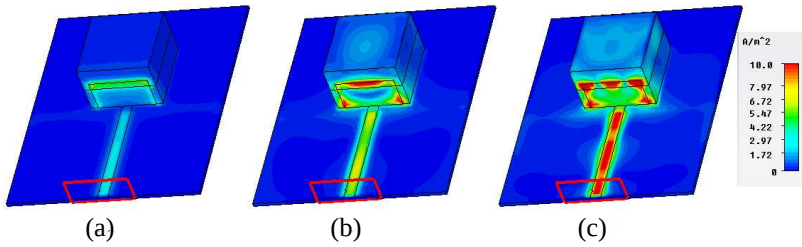

Figure 5. Simulated surface current distributions on the UWBA at (a) 3.5 GHz, (b) 6.5 GHz, (c) 10 GHz.

3.3. Parametric Study

In this section, a parametric study will be carried out on the some antenna parameters to optimize its impedance bandwidth attaining the bandwidth required by the Federal Communications Commission (FCC). This optimization is done by acting on the length of the ground plane lg, the length lp and width wp of the rectangular patch feed.

The effect of the ground plane length on the reflection coefficient for the proposed stacked DRA is shown in Figure 6. It can be seen that the ground plane length lg is very critical parameter on the antenna impedance bandwidth. By increasing the parameter lg the impedance matching becomes poor at low frequencies and vice versa. The optimized value for this parameter is $lg = 16$ mm.

Another parametric study is done on the rectangular patch dimensions. It is clearly observed from Figure 7, that the decrease of the patch length lp provides reduced impedance bandwidth. In addition, reflection coefficients for different patch width wp are presented in Figure 8. It can be seen that the optimal value of the patch width is $wp = 11$ mm.

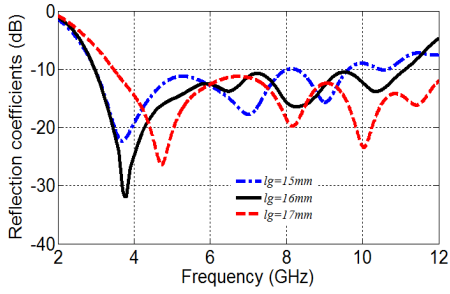

Figure 6. Effect of the ground-plane length lg on reflection coefficient.

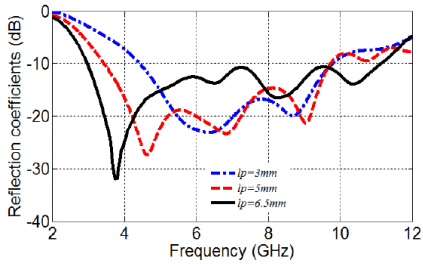

Figure 7. Effect of the rectangular patch length *lp* on reflection coefficient.

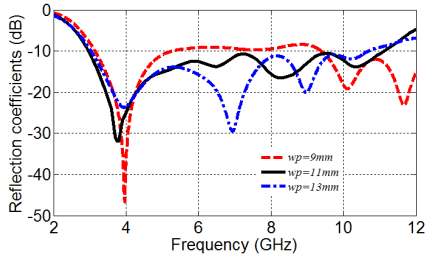

Figure 8. Effect of the rectangular patch width *wp* on reflection coefficient.

4. CONCLUSION

A rectangular stacked dielectric resonator antenna excited by rectangular patch has been numerically analyzed and designed using the FDTD method, Ansoft HFSS software and CST Microwave Studio simulator. The numerical results show that the proposed antenna provides a 3–11 GHz impedance bandwidth and has almost stable radiation patterns with a bidirectional radiation characteristic in the *E*-plane and an omnidirectional in the *H*-plane. Furthermore, the FDTD computed and simulated results are in a good agreement. With these features, the proposed antenna can be a suitable candidate for ultra wideband systems.

REFERENCES

1. Shum, S. M. and K. M. Luk, "Stacked annular-ring dielectric resonator antenna excited by axi-symmetric coaxial probe," *IEEE Trans. Antennas Propagat.*, Vol. 43, 889–892, 1995.
2. Walsh, A. G., S. D. Young, and S. A. Long, "An investigation of stacked and embedded cylindrical dielectric resonator antennas," *IEEE Antennas Wireless Propag. Lett.*, Vol. 5, 130–133, 2006.
3. Denidni, T. A. and Q. Rao, "Hybrid dielectric resonator antennas with radiating slot for dual-frequency operation," *IEEE Antennas Wireless Propag. Lett.*, Vol. 3, 320–323, 2004.
4. Kishk, A. A., Y. Yin, and A. W. Glisson, "Conical dielectric resonator antennas for wideband applications," *IEEE Trans. Antennas Propagat.*, Vol. 50, 469–474, 2002.

5. Kishk, A. A., "Wideband dielectric resonator antenna in a truncated tetrahedron form excited by a coaxial probe," *IEEE Trans. Antennas Propagat.*, Vol. 51, 2907–2912, 2003.
6. Vijumon, P. V., S. K. Menon, M. N. Suma, B. Lehakumari, M. T. Sebastian, and P. Mohanan, "Broadband elliptical dielectric resonator antenna," *Microw. Opt. Technol. Lett.*, Vol. 48, 65–67, 2006.
7. Chair, R., A. A. Kishk, and K. F. Lee, "Wideband stair-shaped dielectric resonator antennas," *IET Microw. Antennas Propag.*, Vol. 1, 299–305, 2007.
8. Liang, X. L. and T. A. Denidni, "H-shaped dielectric resonator antenna for wideband applications," *IEEE Antennas Wireless Propag. Lett.*, Vol. 7, 163–166, 2008.
9. Khalily, M., M. K. A. Rahim, A. A. Kishk, and S. Danesh, "Wideband, P-shaped dielectric resonator antenna," *Radioengineering*, Vol. 22, 146–150, 2013.
10. Ammann, M. J. and Z. N. Chen, "Wideband monopole antennas for multiband wireless systems," *IEEE Antennas Propag. Mag.*, Vol. 45, 146–150, 2003.
11. Liang, J., C. C. Chiau, X. Chen, and C. G. Parini, "Study of a printed circular disc monopole antenna for uwb systems," *IEEE Trans. Antennas Propagat.*, Vol. 53, 3500–3504, 2005.
12. Messaoudene, I., T. A. Denidni, and A. Benghalia, "Experimental investigations of ultra-wideband antenna integrated with dielectric resonator antenna for cognitive radio applications," *Progress In Electromagnetics Research C*, Vol. 45, 33–42, 2013.
13. Augustin, G. and T. A. Denidni, "Coplanar waveguide-fed uniplanar trapezoidal antenna with linear and circular polarization," *IEEE Trans. Antennas Propagat.*, Vol. 60, 2522–2526, 2012.
14. Chair, R., A. Kishk, and K. F. Lee, "Ultrawide-band coplanar waveguide fed rectangular slot antenna," *IEEE Antennas Wireless. Propag. Lett.*, Vol. 3, 227–229, 2004.
15. Liu, Y., K. L. Lau, and C. H. A. Chan, "Circular microstrip-fed single-layer single-slot antenna for multi-band mobile communications," *Micro. Opt. Technol. Lett.*, Vol. 37, 59–62, 2003.
16. Chen, H. D., "Broadband CPW-fed square slot antenna with a widened tuning stub," *IEEE Trans. Antennas Propagat.*, Vol. 51, 1982–1986, 2003.

17. Ahmed, O. M. H., A. R. Sebak, and T. A. Denidni, "Size reduction and bandwidth enhancement of a UWB hybrid dielectric resonator antenna for short-range wireless communications," *Progress In Electromagnetics Research Letters*, Vol. 19, 19–30, 2010.
18. Ryu, K. S. and A. Kishk, "Ultra-wideband dielectric resonator antenna with broadside patterns mounted on a vertical ground plane edge," *IEEE Trans. Antennas Propagat.*, Vol. 58, 1047–1053, 2010.
19. Ryu, K. S. and A. Kishk, "UWB dielectric resonator antenna having consistent omni-directional pattern and low cross-polarization characteristics," *IEEE Trans. Antennas Propagat.*, Vol. 59, 1403–1408, 2011.
20. Niroo-Jazi, M. and T. A. Denidni, "Experimental investigations of a novel ultra-wideband dielectric resonator antenna with rejection band using hybrid techniques," *IEEE Antennas Wireless Propag. Lett.*, Vol. 11, 492–495, 2012.
21. Petosa, A., *Dielectric Resonator Antenna Handbook*, Artech House, Norwood, MA, 2007.
22. Sollivan, D. M., *Electromagnetic Simulation Using the FDTD Method*, IEEE Press, Piscataway, NJ, 2000.
23. Tavlove, A. and C. Hagness, *Computational Electrodynamics: The Finite Difference Time Domain Method*, 2nd Edition, Artech House, 2000.
24. Roden J. and S. Gedney, "Convolution PML (CPML): An efficient FDTD implementation of the CFS-PML for arbitrary media," *Micro. Opt. Technol. Lett.*, Vol. 27, 334–339, 2000.
25. Elsherbeni, A. and V. Demir, *The Finite-difference Time-domain Method for Electromagnetics with Matlab Simulations*, SciTech Publishing, 2009.